Title

PROJECTION-SPACE ITERATIVE INTERPOLATION FOR LIMITED-ANGLE TOMOGRAPHY IN PARALLEL- AND FAN-BEAM GEOMETRY. PART I

Authors

Heiskanen, K.
Wang, J.J.
Perez-Mendez, V.

Publication Date

1987-05-01

LBL-23505
UC-48

Lawrence Berkeley Laboratory
UNIVERSITY OF CALIFORNIA

Physics Division

PROJECTION-SPACE ITERATIVE INTERPOLATION FOR LIMITED-ANGLE TOMOGRAPHY IN PARALLEL- AND FAN-BEAM GEOMETRY. PART I.

K. Heiskanen, J.-J. Wang, and V. Perez-Mendez

May 1987

Prepared for the U.S. Department of Energy under Contract DE-AC03-76SF00098

DISCLAIMER

LBL-23505

Projection-Space Iterative Interpolation for Limited-Angle Tomography in Parallel- and Fan-Beam Geometry. Part I.

Kaarlo Heiskanen, Jong-Jin Wang,* and V. Perez-Mendez
Lawrence Berkeley Laboratory, University of California
Berkeley, California 94720

Abstract

In computed tomography one reconstructs the image of an object from its projections. The limited-angle tomography problem arises when the number of projections available is too small, or the projections are not obtained from all angles around the object, evenly enough distributed. Such is the case, when the object moves while the projections are measured, for example CT - scanning the beating heart. Recently Kim et al. introduced a new algorithm, the projection-space iterative reconstruction-reprojection (PSIRR), for estimating the missing projection data from the known data. Their method is valid for parallel-beam projections only. In this paper their method is further modified and discussed. A similar iterative interpolation algorithm is derived for estimating missing projection data in fan-beam geometry.

1. Introduction

The limited angle problem in computed tomography arises, when the projections cannot be properly measured, perhaps because of the geometric configuration of the scanning device or the object, or the movements of the object during the scan, (such as imaging the heart). Generally the difficulties are more severe if the data are missing in a large sector of contiguous view angles, than if the data are missing in smaller sectors distributed around the whole 360°. In imaging the heart the latter case is encountered. The mathematical work on limited-angle problem has generally been focused on the case of missing data in a sector of contiguous view angles, and in parallel-beam geometry only (see papers by Davison and Grunbaum[1,2] and Louis[3]).

The Gerschberg-Papoulis iteration[4,5] was originally derived and proved for the extrapolation of band-limited one-dimensional signals, and later generalized to two-dimensional images in an application to tomography in parallel-beam geometry. A rigorous mathematical proof of convergence in the two-dimensional case, when the measurement data is obtained as divergent-beam projections, is yet to be done, however. While the proof in the parallel-beam geometry can take advantage of the projection or central-slice theorem, a similar theorem does not exist in the fan-beam geometry. In practice, a modified Gerschberg-Papoulis type iteration - without the corrections in the Fourier-plane – has been successfully employed in fan-beam geometry by a number of researchers.[6,7,8]

In the original Gerschberg-Papoulis iteration, as applied to image reconstruction from projections, one iterates between the image of the object and its two-dimensional Fourier-transform. At each step a correction is made. In the image space the correction includes applying a priori knowledge of the non-negativity and upper bound of the object density, as well as of the limits of its extent. Then the 2-D Fourier-transform of the image is calculated; the Fourier-transform

* Present address: Tsinghua University, Beijing, China

is corrected applying the projection-theorem at the known projections, but leaving the Fourier-transform as it is in other parts. Inverse Fourier-transform gives a new image estimate. A modification, the iterative reconstruction-reprojection algorithm (IRR) operates in the object and projection spaces: at each iteration step, the corrections are done on the image, and then new simulated projections at those view angles, where original data is missing, are obtained by mathematically calculating the line-integrals through the (discrete) image. Then a reconstruction algorithm is applied to obtain a new image estimate.

The reconstruction of the image using the standard backprojection-of-filtered projections includes in principle two operations: i) filtering the projection data, and ii) the backprojection integral over the view angles. The projections of a (continuous) object are obtained using the Radon-transform.

IRR algorithm suffers from the fact that both the reprojection and the image reconstruction require interpolations, and the interpolation errors accumulate during iterations. This often may cause the iteration to diverge after a few steps. Also, when the measurement data is noisy, the effect of noise accumulates in the iterations. Recently, Kim et al. introduced a new algorithm that combines the image reconstruction and the reprojection into one single formula, which eliminates the interpolations[9]. Their formula, the projection space iterative reconstruction-reprojection in projection-space (PSIRR), is valid for parallel-beam projections only. In this paper some modifications of the method of Kim et al. are presented and discussed. Then a formula for projection-space-iterative-reconstruction-reprojection in fan-beam geometry (PSIRRFAN) is derived. Similarly to the parallel-beam case, the formula combines the fan-beam Radon-transform, and the backprojection-of-filtered-projections method for fan-beams into one integral. PSIRRFAN can be used to estimate missing fan-beam projection data through iterative interpolations on the known projection data. Computer simulations, the results of which will be published in a successor paper, have shown PSIRR and PSIRRFAN to converge rapidly, even when up to 70....80% of the projection data is missing, and the known data includes noise. In no tests did the PSIRRFAN iteration diverge.

2. Projection–Space Interpolation Formulas

2.1 The Projection Geometries

The parallel-beam projections $p(l,\theta)$ of an object $f(x,y)$ are obtained from the Radon transform of the object, which is a line-integral along a straight line (see Fig. 1.a):

$$p(l,\theta) \equiv \int_{A}\int_{(x,y)} f(x,y)\delta[l - x\cos\theta - y\sin\theta]dxdy \equiv$$

$$\int_{t_{min}(l,\theta)}^{t_{max}(l,\theta)} f(l\cos\theta + t\sin\theta, l\sin\theta - t\cos\theta)dt \qquad (1)$$

where $A(x,y)$ is the area of support of the object: $f(x,y) \neq 0$ for $(x,y)\epsilon A(x,y)$

- l is the distance of the line from the origin
- θ is the angle between x-axis and the normal of the line
- t_{max}, t_{min} indicate the size of the object along the line.

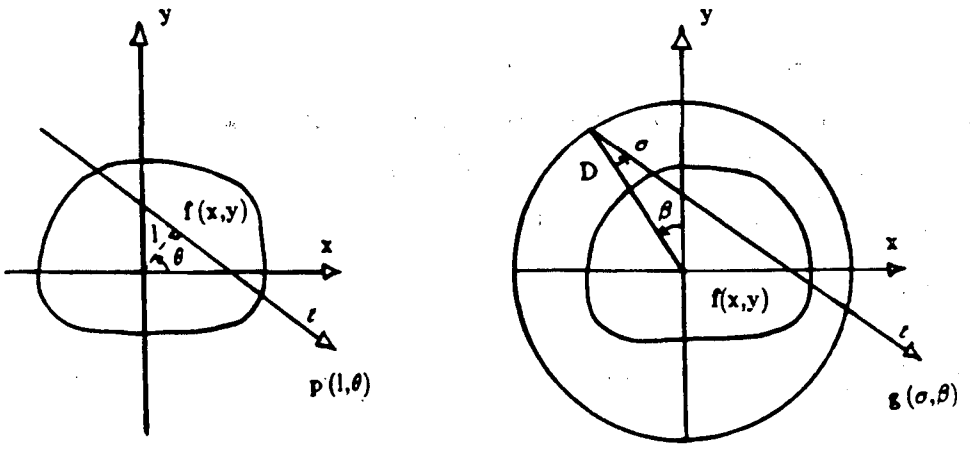

Fig. 1.a) Parallel-beam geometry. b) Fan-beam geometry.

The fan-beam projections $g(\sigma,\beta)$ of an object f(x,y) are obtained from a modification of the Radon-transform, sometimes called the x-ray transform or the divergent-beam Radon-transform (see Fig. 1b):

$$g(\sigma,\beta) = \int_{A\,(x,y)} \int f(x,y)\delta[D\sin\sigma - x\cos(\sigma+\beta) - y\sin(\sigma+\beta)]dxdy$$

$$= \int_{t_{min}(\sigma,\beta)}^{t_{max}(\sigma,\beta)} f[-D\sin\beta + t\sin(\sigma+\beta),\ D\cos\beta - t\cos(\sigma+\beta)]dt \qquad (2)$$

where A (x,y) is the area of support of f(x,y): $f(x,y) \neq 0$ for $(x,y)\epsilon A$ (x,y), $= 0$ elsewhere.

β is the view angle that defines the location of the (x-ray) source: $\beta\epsilon[0, 2\pi]$.

σ is the fan-angle that specifies an individual ray, $\sigma\epsilon(-\frac{\pi}{2},\frac{\pi}{2})$.

D is the distance of the (x-ray) source from the origin.

$t_{max}^{(\sigma,\beta)}$ and $t_{min}^{(\sigma,\beta)}$ indicate the extent of the object along the ray (σ,β) (see Fig. 1b.).

The fan-beam projection is just a line-integral, with the line labeled with parameters D ,σ and β, instead of l and θ. These parameters give the equation of the exactly same line, when $l = D\sin\sigma$, and $\theta = \sigma+\beta$. In that case the projections $p(l,\theta)$ and $g(\sigma,\beta)$ are identical:

$$g(\sigma,\beta) \equiv p(l,\theta) \quad \text{for} \quad l = D\sin\sigma,\ \theta = \sigma+\beta. \qquad (3)$$

2.2 The Parallel-Beam Geometry

The most widely used method for image reconstruction, i.e., obtaining the inverse Radon-transform, probably is the backprojection-of-filtered-projections algorithm, which consists of two steps, filtering and backprojection:

i) filtering (for θ = const.):

$$\tilde{p}(l,\theta) = p(l,\theta) * F^{-1}\{\,|\omega_l|\,\} = F^{-1}\{\,|\omega_l|\ F\{p(l,\theta)\}\} \qquad (4)$$

where

* denotes convolution with respect to l.

F^{-1} denotes the inverse Fourier-transform with respect to ω_l.

F denotes the Fourier-transform with respect to l.

$\tilde{p}(l,\theta)$ denotes the filtered projection.

ii) backprojection:

$$f(x,y) = \int_0^{\pi} \tilde{p}(x\cos\theta + y\sin\theta, \theta)d\theta \tag{5}$$

In the IRR-algorithm the discrete versions of (1) ... (3) are repeated in an iterative form, which requires interpolation in (1) and (3). Kim et al. developed their method substituting (4) and (5) into (1), and assuming the area of support A(x,y) of the object f(x,y) to be a circle of radius L. However, it is easy to incorporate a priori knowledge of the size of the object in $t_{min}(l,\theta)$ and $t_{max}(l,\theta)$. Then we get for a projection missing at (l_m,θ_n) after the i^{th} iteration:

$$p^{i+1}(l_m,\theta_n) = \int_{t_{min}(l_m,\theta_n)}^{t_{max}(l_m,\theta_n)} f^i(l_m\cos\theta_n + t\sin\theta_n, l_m\sin\theta_n - t\cos\theta_n)dt$$

$$= \int_{t_{min}(l_m,\theta_n)}^{t_{max}(l_m,\theta_n)} \int_0^{\pi} \tilde{p}^i[(l_m\cos\theta_n + t\sin\theta_n)\cos\theta + (l_m\sin\theta_n - t\cos\theta_n)\sin\theta, \theta]d\theta dt$$

$$= \int_{t_{min}(l_m,\theta_n)}^{t_{max}(l_m,\theta_n)} \int_0^{\pi} \tilde{p}^i[l_m\cos(\theta_n - \theta) + t\sin(\theta_n - \theta), \theta]d\theta dt \tag{6}$$

Introducing a new variable, $t' = l_m\cos(\theta_n - \theta) + t\sin(\theta_n - \theta)$, and changing the order of integration one gets the PSIRR-formula of Kim et al., with a priori information used in the limits of integration:

$$p^{i+1}(l_m,\theta_n) = \int_0^{\pi} \frac{1}{\sin(\theta_n - \theta)} \int_{t'_{min}(l_m,\theta_n,\theta)}^{t'_{max}(l_m,\theta_n,\theta)} \tilde{p}^i(t', \theta)dt'd\theta \tag{7}$$

where:

$$t'_{min}(l_m,\theta_n,\theta) = l_m\cos(\theta_n - \theta) + t_{min}(l_m,\theta_n)\sin(\theta_n - \theta)$$

$$t'_{max}(l_m,\theta_n,\theta) = l_m\cos(\theta_n - \theta) + t_{max}(l_m,\theta_n)\sin(\theta_n - \theta)$$

(7) gives an iterative interpolation formula for approximating the values of missing projections $p(l_m,\theta_n)$ for any l_m and θ_n, from the known projection values. No interpolation is necessary, when the formula is written in a discrete from. (Note, however, the singularity at $\theta = \theta_n$, which needs to be avoided in numerical calculations and that at $\theta = \theta_n$, $t'_{min} = t'_{max}$.) In [9], the convergence of (7) with noise added in the data, is shown in computer simulations.

We can modify (7) further including the integration over t′ already into the filter function.

Consider the integral

$$r(t) = \int_{-\infty}^{t} h(t')\, dt'.$$

We know that [5, p.40] if $H(\omega) = F\, h(t)$ then

$$F\, r(t) = R(\omega) = [\pi\delta(\omega) + (i\omega)^{-1}] \tag{8}$$

and the integral over t′ in (7) becomes

$$\int_{t'_{min}}^{t'_{max}} \tilde{p}^i(t', \theta)dt' = \tilde{p}^i_1(t'_{max}, \theta) - \tilde{p}^i_1(t'_{min}, \theta) \tag{9}$$

$$\text{where } \tilde{p}^i_1(t', \theta) = F^{-1}\left\{R(\omega)F\left\{p^i(t', \theta)\right\}\right\}. \tag{10}$$

Eq. (7) can then be written in the simple form:

$$p^{i+1}(l_m, \theta_n) = \int_0^{\pi} \frac{\tilde{p}^i_1(t'_{max}, \theta) - \tilde{p}^i_1(t'_{min}, \theta)}{\sin(\theta_n - \theta)}\, d\theta \tag{11}$$

where

$$t'_{max} = l_m(\theta_n - \theta) + t_{max}(l_m,\theta_n)\sin(\theta_n - \theta)$$

$$t'_{min} = l_m\cos(\theta_n - \theta) + t_{min}(l_m,\theta_n)\sin(\theta_n - \theta)$$

and $\tilde{p}^i_1$ is obtained from (10).

One can derive yet another form of PSIRR, if one uses the Hilbert-transform version of the inverse Radon-transform:

$$p^{i+1}(l_m,\theta_n) = \int_0^{\pi}\int_{-L}^{L} \frac{p^i(l,\theta)}{\sin(\theta_n-\theta)} \left[\frac{1}{t'_{max}(l_m,\theta_n,\theta) - l} - \frac{1}{t'_{min}(l_m,\theta_n,\theta) - l}\right] dl\, d\theta \tag{11′}$$

This form of PSIRR is numerically unstable, however, because of the singularities in the integrand, as is typical of the Hilbert-transform.

The geometric meaning of PSIRR is explained in Fig. 2.

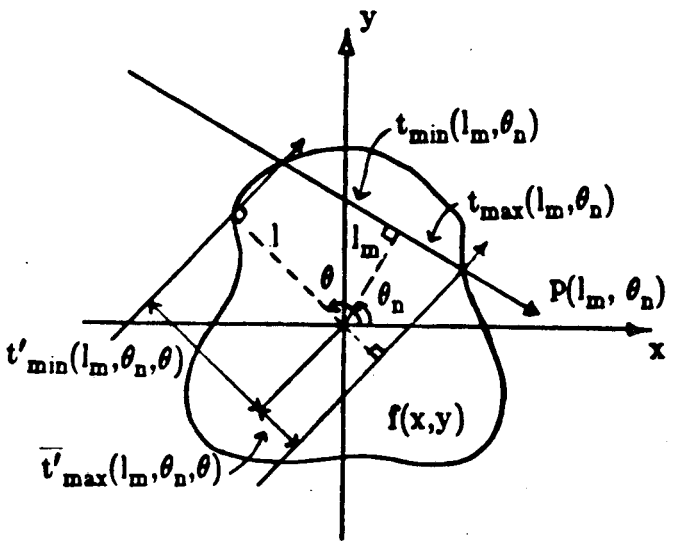

Fig. 2 The geometric meaning of PSIRR.

In (7), for each value of θ, one integrates over the filtered projection $\tilde{p}(l,\theta)$ between t'_{min} and t'_{max} which, as indicated if Fig. 2, depend directly on the known outer boundary of the object as given by t_{min},t_{max}. Each sum is multiplied by the weight $\frac{1}{\sin(\theta_n - \theta)}$, the absolute magnitude of which is always greater than or equal to one.

PSIRR can be written in operator form as:

$$p^{i+1}(l,\theta) = R\left\{f^i(x,y)\right\} = RR^{-1}\left\{p^i(l,\theta)\right\}$$

where R denotes the Radon-transform and R^{-1} its inverse. For PSIRR the operator RR^{-1} is modified and simplified. RR^{-1} includes the filtering selected for the reconstruction; obviously the faster the convergence of PSIRR, the better the filter selection was. Thus PSIRR offers a simple, quantitative way of evaluating the quality of one's filter selection for any particular set of projection data.

One of the difficulties in Gerschberg-Papoulis-type iterative reconstruction-reprojection algorithms has been how to know when to end the iterations. In PSIRR this problem is simply overcome, as one can use PSIRR to calculate estimates at a number of projections, which actually were measured, and use this error behavior as the criteria for iterations.

Obviously PSIRR achieves the best results when the measured data is available as complete projections (see Fig. 3a), which are more or less evenly distributed over the range of $\theta\epsilon[,\pi]$. The convergence is slower if the missing data belong to one sector of contiguous angles; then the ill-posed nature of the limited-angle data is more pronounced (Fig. 3b). In some applications the missing projections are located on sinusoidal curve(s) in the projection space (Fig. 3c, d) In this case all projections are influenced by the missing data, and thus all the filtered projections required in PSIRR will be distorted and need to be updated at each iteration cycle.

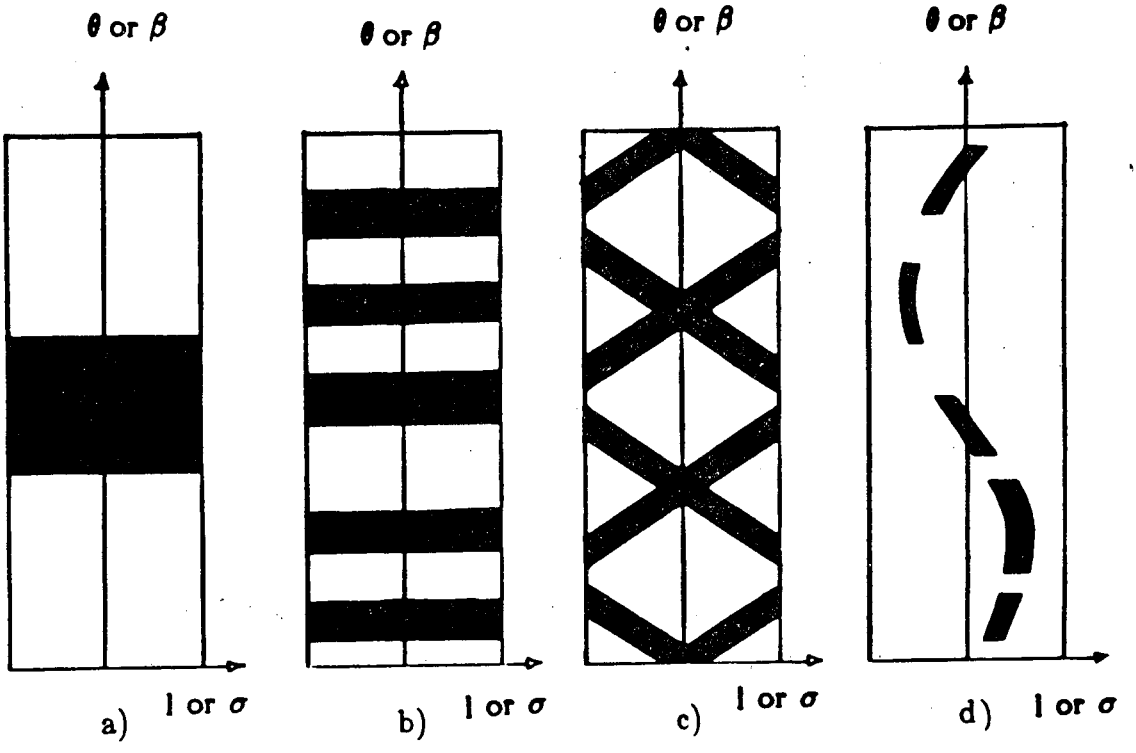

Fig. 3. Examples of missing projection data. a) Complete projections missing in a sector of contiguous view angles, $\theta,<\theta<\theta_2$. This is the standard "limited-angle" situation. b) Complete projections missing at random view angles, or otherwise distributed over the whole range $[0, \pi]$ of the view angle. This kind of situation may arise, for example, in EKG-gated imaging of a moving heart. c) Missing projection data distributed over sinusoidal curves. This situation will arise, when using a fixed system of six, flat detectors as in some positron emission tomography designs. d) Missing projection data distributed over one sinusoidal curve Examples of the latter case include imaging a moving heart, if the missing data consist only of the line-integrals that pass through the heart

2.3. The fan-beam projections

As in the case of parallel-beam projections, the most widely used image reconstruction method, i.e., obtaining the inverse x-ray transform, is the backprojection-of-filtered projections algorithm [see 10, pp. 400-405]. It has two steps, similarly to the parallel beam case: filtering the projections and backprojection.

i) filtering (for β = const):

$$\tilde{g}(\sigma,\beta) = [D\cos\sigma g(\sigma,\beta)]^* \left[\frac{1}{2}\left(\frac{\sigma}{\sin\sigma}\right)^2 h(\sigma)\right] \tag{12}$$

where * denotes convolution with respect to σ

$h(\sigma) = F^{-1}\left\{ |\omega_\sigma| \right\}$, inverse Fourier-transform of the "magnitude omega" filter.

ii) backprojection:

$$f(x,y) = \int_0^{2\pi} \frac{1}{L^2(x,y,\beta)} \tilde{g}(\sigma,\beta) \Big|_{\sigma = \sigma'(x,y,\beta)} d\beta \tag{13}$$

where:

$L(x,y,\beta)$ is the distance from the source point $(-D\sin\beta, D\cos\beta)$ to the point (x,y)

$\sigma'(x,y\beta)$ is that fan-angle at which the ray from source at $(-D\sin\beta, D\cos\beta)$ passes through the point (x,y).

It can easily be seen that:

$$L^2(x,y,\beta) = D^2 + x^2 + y^2 + 2D(x\sin\beta - y\cos\beta) \tag{14}$$

$$\sigma'(x,y,\beta) = \arctan\left[\frac{x\cos\beta + y\sin\beta}{D + x\sin\beta - y\cos\beta}\right] \tag{15}$$

For the projection-space-iterative-reconstruction-reprojection in fan-beam geometry (PSIRRFAN), equations (12) and (13) are substituted directly into (2) in an iterative form. Thus an estimate of the fan-beam projection $g(\sigma_m,\beta_n)$ at coordinates (σ_m,β_n), after ith iteration, is obtained as:

$$g^{i+1}(\sigma_m,\beta_n) = \int_{tmin(\sigma_m,\beta_n)}^{t_{max}(\sigma_m,\beta_n)} f_i(x(\sigma_m,\beta_n,t),y(\sigma_m,\beta_n,t)dt$$

$$= \int_{t_{min}(\sigma_m,\beta_n)}^{t_{max}(\sigma_m,\beta_n)} \int_0^{2\pi} \frac{1}{L^2(x(\sigma_m,\beta_n,t),y(\sigma_m,\beta_n,t),\beta)} \tilde{g}^i(\sigma,\beta) \Big|_{\sigma = \sigma'(x(\sigma_m,\beta_n,t),y(\sigma_m,\beta_n,t),\beta)} d\beta dt \quad (16)$$

where

$$x(\sigma_m,\beta_n,t) = -D\sin\beta_n + t\sin(\sigma_m + \beta_n) \quad (17)$$

$$y(\sigma_m,\beta_n,t) = D\cos\beta_n - t\cos(\sigma_m + \beta_n)$$

Using the coordinates (17) in (14) and (15) we get:

$$L^2(x(\sigma_m,\beta_n,t),y(\sigma_m,\beta_n,t),\beta) = 2D^2 + t^2 - 2Dt\cos\sigma_m - 2D^2\cos(\beta - \beta_n) + 2Dt\cos(\beta - \beta_n - \sigma_m) \quad (18)$$

$$\sigma'(x(\sigma_m,\beta_n,t),y(\sigma_m,\beta_n,t)\beta) = \arctan\left[\frac{D\sin(\beta - \beta_n) - t\sin(\beta - \beta_n - \sigma_m)}{D - D\cos(\beta - \beta_n) + t\cos(\beta - \beta_n - \sigma_m)}\right] \quad (19)$$

Formula (16), as well as (13), has an inbuilt inaccuracy. In real life one is dealing with discrete data, obtained at discrete values of the fan-angle σ and view angle β. The value of fan-angle σ', as calculated from (15) or (19), does not usually coincide with any of the discrete measurement angles σ, and thus interpolation is necessary. In PSIRRFAN this inaccuracy is removed by a change of variable.

According to (19), let the new variable of integration in (16) be σ'. From (19) we get:

$$t = D\left[\frac{\sin(\beta - \beta_n) - (1 - \cos(\beta - \beta_n))\tan\sigma'}{\sin(\beta - \beta_n - \sigma_m) + \cos(\beta - \beta_n - \sigma_m)\tan\sigma'}\right] \quad (20)$$

$$\frac{dt}{d\sigma'} = \frac{-D(1 + \tan^2\sigma')(\sin\sigma_m + \sin(\beta - \beta_n - \sigma_m))}{[\sin(\beta - \beta_n - \sigma_m) + \cos(\beta - \beta_n - \sigma_m)\tan\sigma']^2} \quad (21)$$

The new limits of integration in (16) are:

$$\sigma'_{max}(\sigma_m,\beta_n,t_{max},\beta) = \arctan\left[\frac{D\sin(\beta - \beta_n) - t_{max}(\sigma_m,\beta_n)\sin(\beta - \beta_n - \sigma_m)}{D(1 - \cos - (\beta - \beta_n) + t_{max}(\sigma_m,\beta_n)\cos(\beta - \beta_n - \sigma_m)}\right] \quad (22)$$

$$\sigma'_{min}(\sigma_m,\beta_n,t_{min},\beta) = \arctan\left[\frac{D\sin(\beta-\beta_n) - t_{min}(\sigma_m,\beta_n)\sin(\beta-\beta_n-\sigma_m)}{D(1-\cos(\beta-\beta_n) + t_{min}(\sigma_m,\beta_n)\cos(\beta-\beta_n-\sigma_m)}\right] \quad (22)$$

A priori information about the size of the object is thus directly included in the limits of integration, σ'_{min} and σ'_{max}.

Next substitute (20) into (18). After lengthy but straightforward trigonometric manipulations, one can show that:

$$\frac{1}{L^2(x(\sigma'),y(\sigma'),\beta)} \cdot \left(\frac{dt}{d\sigma'}\right) = \frac{-1}{D} \cdot \frac{1}{\sin\sigma_m + \sin(\beta-\beta_n-\sigma_m)} \quad (23)$$

i.e. the dependence on σ' cancels out. The change of variables in (16) must be preceded by a change in the order of integration

$$g^{i+1}(\sigma_m,\beta_n) = \int_0^{2\pi}\int_{t_{min}}^{t_{max}} \frac{1}{L^2(x(t),y(t),\beta)}\tilde{g}^i(\sigma,\beta)\Big|_{\sigma=\sigma'} dt\,d\beta$$

$$= \int_0^{2\pi}\int_{\sigma'_{min}}^{\sigma'_{max}} \frac{1}{L^2(x(\sigma'),y(\sigma'),\beta)}\tilde{g}^i(\sigma',\beta)\left(\frac{dt}{d\sigma'}\right)d\sigma'\,d\beta \quad (24)$$

and, substituting (23) into (24) finally gives the PSIRRFAN-formula:

$$g^{i+1}(\sigma_m,\beta_n) = \int_0^{2\pi} \frac{-1}{D}[\sin\sigma_m + \sin(\beta-\beta_n-\sigma_m)]^{-1} \int_{\sigma'_{min}}^{\sigma'_{max}} \tilde{g}^i(\sigma',\beta)d\sigma'\,d\beta \quad (25)$$

where $g^i(\sigma', \beta)$ is calculated from (12), for any i, and σ'_{min}, σ'_{max} are given in (22).

PSIRRFAN, as given by eq. (25), is an iterative formula. The iteration starts from the known projection data, where the missing data can be set to zero originally, or for faster initial convergence, to some positive starting values. Each projection is filtered using the standard filtering methods used in the reconstruction of images. The filtering typically includes a window or smoothing window function.

Each filtered projection is integrated with respect to fan-angle, between limits σ'_{min} and σ'_{max}. These limits of integration depend on the angles β_m and σ_n of the missing ray, and the extent of the object along the missing ray, t_{min} and t_{max} (see eq. (22). The projection data $g(\sigma,\beta)$ is measured at discrete points σ_i, β_j and the limits of integration, σ'_{min} and σ'_{max}, will have values that fall somewhere between two measurement points σ_i,σ_{i+1}. This is a very minor inaccuracy and does not necessitate interpolation.

The limits of integration, σ'_{min} and σ'_{max}, include a priori information of the extent of the object directly, in t_{min} and t_{max}. The other a priori information about the object, namely

positivity and upper bound of density f(x,y), cannot be used as directly. We can demand, however, that the projection values are to be non-negative and less than some known or guessed maximum value. Also, for any ray that does not go through the object, the projection must be zero. Any assumptions of the smoothness of the object are included in the filter selection.

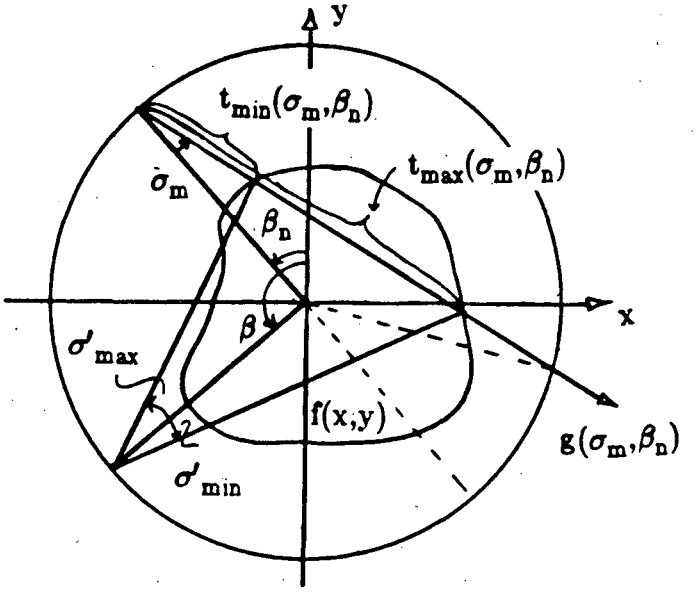

Fig. 4. the geometric meaning of Eq. (25). The ray symmetric to $g(\sigma_m,\beta_n)$ is $g(-\sigma_m,\beta_n + \pi + 2\sigma_m)$.

Fig. 4. shows the geometric interpretation of eq. (25).

The weight function is:

$$W(\sigma_m,\beta_n,\beta) = \frac{1}{\sin\sigma_m + \sin(\beta - \beta_n - \sigma_m)}$$

Since W comes from $W = \frac{1}{L^2} \cdot \left(\frac{dt}{d\sigma'}\right)$, and $\frac{1}{L^2}$ is positive, the sign of W is defined by the sign of $\left(\frac{dt}{d\sigma'}\right)$. For $\left(\frac{dt}{d\sigma'}\right)$ negative, W is negative, but also σ_{min} (associated with t_{min}) is larger than σ'_{max} (associated with t_{max}). This is evident in Fig. 4. Thus, when the limits of integration, σ_{min} and σ_{max} are changed over, the product of the weight function and the integral becomes positive.

There are two singularities in W, namely $\beta = \beta_n$, which represents the missing ray itself, and $\beta = \beta_n + 2\sigma_m + \pi$, which represents the symmetric ray (see Fig. 4.). At these singularities, $\sigma'_{min} = \sigma'_{max}$, and the inner integral becomes zero. If the symmetric projection $g(-\sigma_m,\beta_n + 2\sigma_m + \pi)$ of the missing projection $g(\sigma_m,\beta_n)$ was measured, we substitute its value directly for $g(\sigma_m,\beta_n)$; if it wasn't, we skip over the singularity at $\beta = \beta_n + 2\sigma_m + \pi$. (Substituting the symmetric projection for the missing one is sometimes called a "reflection method" [7].

In Fig. 5a.).....d) some examples of the values that the weight function and the limits of integration that σ'_{min} and σ'_{max}, may assume are given. The limits of integration depend on the size of the object f(x,y); here for simplicity, the object was assumed to be circular with radius 0.75 times the radius of the x-ray source path. The curves are evaluated in terms of $\Delta\beta = \beta - \beta_n$ where $\Delta\beta = 0.....\pm,2\pi$. The figures correspond to values $\sigma_m = 0°$, $20°$ and $\pm 30°$.

The highest value of the weight function depends on the sampling rate in the angle β. In Fig. 2 a sampling interval of $1°$ was used. The maximum value of the weight function then is around 20; then the integration interval, $\sigma'_{max} - \sigma'_{min}$, approaches zero however.

Although PSIRRFAN, in principle, is similar to PSIRR, there are some differences. One arises from the fact that the symmetric rays are distributed differently in the fan-beam geometry than in the parallel-beam geometry, and typically for any missing fan-beam projection, some symmetric rays were measured in other projections. Thus the distribution of the missing projections over the range of $\beta\epsilon[0,2\pi)$ carries a different significance. Computer simulations are under way in which the the influence of the distribution of the missing projections will be established.

3. Discussion

The iterative reconstruction-reprojection (IRR) algorithm, which originated from the Gerschberg-Papoulis algorithm, has been applied by several authors in limited-angle tomography, both in parallel- and fan-beam geometry. In principle, IRR works, but in practice there are several limitations and difficulties involved. Especially : i) the convergence of IRR is sensitive to noise in the measurement data, ii) interpolation and roundoff errors may tend to accumulate during the iterations, and together with the influence of noise, often cause the iteration to diverge after a few iterations, iii) the computational demands can be overwhelming, when the number of pixels in the image is large, iv) there is no simple criteria for stopping the iteration, as the correct image, of course, is not known.

PSIRR (and PSIRRFAN) remove most of these basic weaknesses of IRR. The interpolations necessary in both the reconstruction and the reprojection stage of IRR are not needed in PSIRR. The computational requirement in PSIRR is related to the number of missing projections, not to the - usually much larger - number of pixels in the image, as in IRR. (Actually, evaluating the estimated value of one missing projection, using PSIRR, requires roughly the same computational effort as reconstructing the value of the image in one pixel.) Also, PSIRR includes naturally a criteria for stopping the iteration, as the algorithm can be used to obtain estimated values for projections for which the measured values also exist.

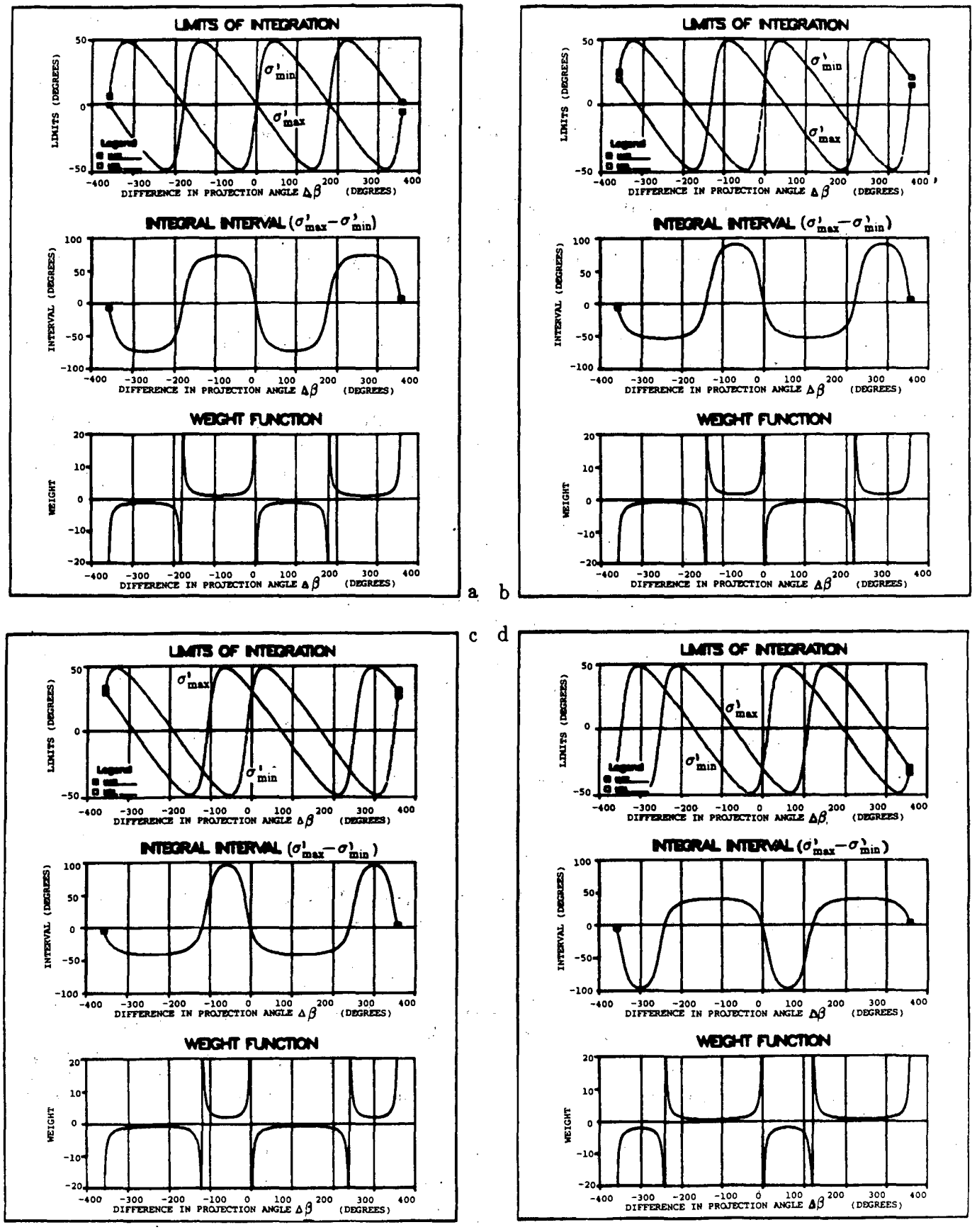

Fig. 5. The limits of inner integration, the integral interval (upper limit-lower limit), the weight function according to the difference between β and β_n in the case of R/D = 0.75 and (a) $\sigma_m = 0$, (b) $\sigma_m =$ 20 degrees, (c) $\sigma_m =$ 30 degrees, (d) $\sigma_m =$ -30 degrees.

PSIRR (and PSIRRFAN) is a two dimensional interpolation in the projection space. As an interpolation method, PSIRR differs from other methods, being based directly on the properties of the Radon-transform and its inverse. For interpolation, PSIRR uses all the relevant projection data, not just some nearest neighbor data. Also, PSIRR is used iteratively, unlike other interpolation methods.

Because both PSIRR and PSIRRFAN operate on filtered projections, they are best suitable for situations where at each view angle, the projection is either completely known or completely missing. If the missing data is distributed so that at each view angle some rays are missing, the corresponding filtered data cannot be calculated accurately.

The influence of noise, as well as the distribution of the missing data, on the converge and accuracy of PSIRR and PSIRRFAN will be assessed in a future paper.

† This work was supported by the Director, Office of Energy Research, Office of High Energy and Nuclear Physics, Division of High Energy Physics, and Office of Health and Environmental Research, Division of Physical and Technological Research of the U.S. Department of Energy under contract #DE-AC03-76SF00098.

References

1. M.E. Davison, The Ill-Conditioned Nature of the Limited Angle Tomography Problem, SIAM J. Appl. Math. **43**, pp. 428-448 (1983).
2. M.E. Davison, F.A. Grunbaum, Tomographic Reconstruction with Arbitrary Directions, Commun. Pure Appl. Math. **34**, pp. 77-120 (1981).
3. A.K. Louis, Incomplete Data Problems in X-Ray Computerized Tomography. Numer. Math. **48**, no. 3, pp. 251-262 (1986).
4. R.W. Gerschberg, Super-Resolutions Through Error Energy Reduction, Optica Acta, vol. **21**, no. 9, pp. 709-710 (1974).
5. A. Papoulis, A New Algorithm in Spectral Analysis and Band-Limited Extrapolation, IEEE Trans. Circuits Syst., vol. **CAS-22**, pp. 735-742 (1975).
6. K.C. Tam, V. Perez-Mendez, Limited-Angle three-Dimensional Reconstructions Using Fourier Transform Iterations and Radon Transform Iterations, Optical Eng., vol. **20**, no. 4, pp. 586-589 (1981).
7. M. Nassi, W.R. Brody, B.P. Medoff, A. Macovski, Iterative Reconstruction-Reprojection: An Algorithm for Limited Data Cardiac-Computed Tomography, IEEE Trans. Biomed. Eng., vol. **BME-29**, no. 5, pp. 333-341 (1982).
8. P.B. Heffernan, R.A. Robb, Image reconstruction from Incomplete Projection Data: Iterative Reconstruction-Reprojection Techniques, IEEE Trans. Biomed. Eng., vol. **MBE-30**, no. 12, pp. 838-841 (1983).
9. J.H. Kim, K.Y. Kwak, S.B. Park, Z.H. Cho, Projection Space Iteration Reconstruction-Reprojection, IEEE Trans. Med. Imaging, vol. **M1-4**, no. 3, 139-143 (1985).
10. A. Rosenfeld, A.C. Kak, Digital Picture Processing, 2nd ed., vol. **1**, Academic Press (1982).

LAWRENCE BERKELEY LABORATORY
TECHNICAL INFORMATION DEPARTMENT
UNIVERSITY OF CALIFORNIA
BERKELEY, CALIFORNIA 94720